nature reviews materials

https://doi.org/10.1038/s41578-025-00781-7

Perspective

Check for updates

Resilience pathways for halide perovskite photovoltaics under temperature cycling

Luyan Wu[1,2,13], Shuaifeng Hu[3,13], Feng Yang[4,5,13], Guixiang Li[1,6,7] ✉, Junke Wang[3], Weiwei Zuo[8], José J. Jerónimo-Rendon[8], Silver-Hamill Turren-Cruz[9], Michele Saba[2], Michael Saliba[8,10], Mohammad Khaja Nazeeruddin[6], Jorge Pascual[11] ✉, Meng Li[4] ✉ & Antonio Abate[1,12] ✉

Abstract

Metal-halide perovskite solar cells have achieved power conversion efficiencies comparable to those of silicon photovoltaic (PV) devices, approaching 27% for single-junction devices. The durability of the devices, however, lags far behind their performance. Their practical implementation implies the subjection of the material and devices to temperature cycles of varying intensity, driven by diurnal cycles or geographical characteristics. Thus, it is vital to develop devices that are resilient to temperature cycling. This Perspective analyses the behaviour of perovskite devices under temperature cycling. We discuss the crystallographic structural evolution of the perovskite layer, reactions and/or interactions among stacked layers, PV properties and photocatalysed thermal reactions. We highlight effective strategies for improving stability under temperature cycling, such as enhancing material crystallinity or relieving interlayer thermal stress using buffer layers. Additionally, we outline existing standards and protocols for temperature cycling testing and we propose a unified approach that could facilitate valuable cross-study comparisons among scientific and industrial research laboratories. Finally, we share our outlook on strategies to develop perovskite PV devices with exceptional real-world operating stability.

Sections

Introduction

Impacts of temperature cycling on perovskite photovoltaic devices

Strategies to enhance the resilience of perovskite photovoltaics to temperature cycling

Photovoltaic performance under real-world diurnal cycles

Stability assessment protocols

Outlook

A full list of affiliations appears at the end of the paper. ✉e-mail: guixiang.li.gl@gmail.com; jpascual1992@gmail.com; mengli@henu.edu.cn; antonio.abate@helmholtz-berlin.de

Introduction

Since their early introduction, metal-halide perovskite solar cells (PSCs) have evolved rapidly owing to their exceptional photovoltaic (PV) properties[1–6] and low-cost solution-based and vacuum-based fabrication[7–10]. The leading power conversion efficiencies (PCEs) of single-junction PSCs now approach 27%[11] (NREL best research-cell efficiency chart) and are on par with those of silicon cells. In tandem PVs, double-junction devices with two stacked photo-absorbers in series could achieve a potential PCE exceeding 45%[12], benefiting from the reduced thermalization loss of the excitons. Owing to the bandgap tunability[13] and ultra-long carrier diffusion length[14] of metal halide perovskites, depositing, for instance, a 1 µm thick layer of perovskite with a bandgap of ~1.7 eV atop a conventional silicon subcell (~1.1 eV) enables PCE of more than 34% in laboratory-scale small cells and of more than 30% in commercial wafer-scale devices. Moreover, monolithic double-junction 'all-perovskite' tandems have achieved PCE values of more than 30%[15]. In principle, multijunction perovskite-based tandems could reach PCE values of more than 50%, constituting the most cost-effective PV products on the market[12]. Efficiency is thus the main asset of PSCs, taking these semiconductors a step closer to practical implementation.

However, perovskite-based materials and devices face stability challenges, primarily related to defect generation, ion migration, phase transitions and interface degradation, raising critical concerns regarding their future practical viability. To date, studies on perovskite device stability have primarily focused on operational stability at room temperature[16,17] or on accelerated ageing[18,19] (for example, under elevated fixed temperature such as +85 °C) to extrapolate the 'potential long-term lifespan'[20–30]. However, during practical operation, PV devices are constantly exposed to temperature changes. Thus, to accurately predict the stability of perovskite PV devices under practical operation[31], they need to be studied under temperature cycling, which is a condition that is scarcely explored. Variations in temperature exert a critical influence on the structural and chemical changes in the materials, the device structure and the PV performance, which is different from the exposition to fixed temperatures. Thus, understanding the impact of temperature and temperature variations (which we refer to as temperature cycles throughout) on materials and devices, and performing the corresponding stability analysis, is of utmost importance for developing long-term stable perovskite PV technology.

The temperature fluctuates with diurnal cycles, seasonal variations, altitude differences and diverse geographical locations (from the poles to the equator)[32]. For instance, extreme temperature changes (for example, in deserts) pose additional challenges for the implementation of perovskite PVs[33–37]. Other applications, such as extraterrestrial use (for example, in spacecraft, high-altitude pseudo-satellites, international space stations and Mars rovers)[35,38–41], impose even more severe conditions owing to a larger temperature range[31,42,43]. These temperature cycles have a substantial impact on the lifespan of PV devices[44–46], influencing properties such as lattice strain, crystallographic site defects, phase transitions, ion migration and material diffusion between and among the stacked device layers[47–51]. Combined with the influence of photons and other stressors, temperature cycles can accelerate device failure compared with the commonly used elevated constant temperature tests[18,52–54], while also being more representative of the practical outdoor behaviour of the devices[55]. Thus, summarizing and understanding the working and failure mechanisms of perovskites and their devices under thermal cycling is particularly meaningful for the development of commercial perovskite-containing PVs.

In this Perspective, we discuss the importance of temperature cycling when evaluating long-term perovskite PV stability. We aim to emphasize the temperature-variation-induced degradation of PSCs, which is often disregarded in comparison to degradation at elevated temperatures. We present a systematic overview of the structure and performance evolution of perovskite-based PV devices under temperature cycles, and we compare perovskite materials of different bandgaps to highlight the influence of perovskite composition on temperature-variation-induced degradation. We also propose strategies to improve operational stability under temperature cycling, and we recommend suitable protocols for assessing device evolution under extended thermal cycling. Finally, we share our opinions on the future challenges for developing perovskite PV devices resistant to temperature cycles.

Impacts of temperature cycling on perovskite photovoltaic devices

Temperature cycling has different impacts on perovskite materials and PV devices. In the perovskite device stack, the layers most affected by temperature cycling are the perovskite layer and the charge transporting layers (CTLs). In the perovskite layer, phase transitions are temperature-dependent and are strongly influenced by perovskite composition. Temperature cycling might lead to irreversible phase transitions and lattice distortions owing to strain (Fig. 1). In addition, temperature cycling promotes the interaction, diffusion and penetration of perovskite components with the CTLs and its interfaces. Furthermore, dynamic fluctuations in CTLs owing to temperature can exert additional strain on the perovskite layer. Finally, temperature has a direct effect on PV parameters. Although the influence of temperature on PV parameters is usually reversible, consecutive cycling can induce a permanent declining trend in performance.

Impact on the perovskite layer

Temperature cycling has two main consequences in the integrity of the perovskite layer. First, perovskite crystalline phase is dependent on the environment temperature. Therefore, consecutive cycles of temperature will impose successive phase transitions that can lead to irreversible degradation. Second, temperature-driven lattice distortions introduce lattice strain in the films that will accumulate with increased cycling.

Phase transitions. Temperature drives perovskite phase changes by affecting thermal energy, atomic vibration and ionic migration (Fig. 2a). In general, under thermal cycling, two distinct phase transition behaviours impact the performance of the device[56]. The first is a reversible phase transition between the cubic and tetragonal phases, which accounts for variations of properties within a single thermal cycle. The second is an irreversible phase transition, such as the transformation to the hexagonal photoinactive polytype phase (that is, 4H and 6H)[57] and decomposition to PbI_2, which results in continued and unrecoverable degradation of the perovskite and device (Fig. 2b). The tetragonal phase (β-phase) is usually retained in the low-temperature region after multiple thermal cycles[56,58]. Phase transitions are more readily reversible in the out-of-plane direction compared with the in-plane direction, where additional forces are exerted by the substrate. Under such reversible behaviour, device performance is unlikely to experience critical degradation when the temperature returns to normal operating conditions.

In addition, the evolution of the perovskite structure when subjected to temperature cycles strongly depends on the composition of the material. In the archetypical perovskite, $MAPbI_3$, for example, the cubic phase evolves to the tetragonal phase at temperatures below

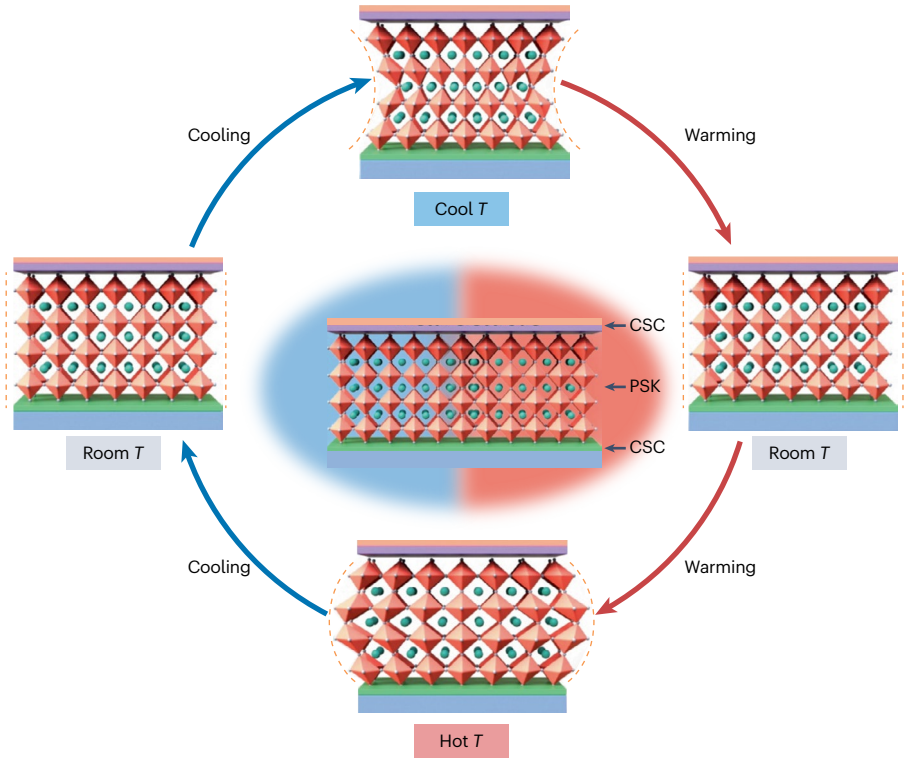

Fig. 1 | The cycling temperature influence on perovskite structure. CSC, charge selective contact; PSK, perovskite; *T*, temperature.

327 K, with a further transition to the orthorhombic phase below 162 K (ref. 59). Meanwhile, when the temperature reaches over 350 K, the thermally induced release of organic cations (MA^+) and vaporization of the amine (MA) lead to the degradation of the perovskite crystal[60,61]. In FAMACs-based perovskite (FA = formamidinium)[62,63], the transition from the original cubic phase to the tetragonal phase occurs at ~240 K, whereas the transition from the tetragonal to the orthorhombic phase does not occur above 100 K. The different phase transition temperatures between these two perovskite compositions suggest that perovskite composition is pivotal in determining its phase transition dynamics. In theory, maintaining the corner-sharing assembly of the perovskite octahedral units in the 3D structure is critical to preserving its optoelectronic properties. This understanding helps deepen insights into the perovskite structure, directly impacting the reliability of the device.

Strain. Beyond phase transitions, continuous lattice distortions can occur throughout the entire temperature cycling process, and the lattice strain has a central role[64,65]. In solar cells, especially tandem cells, the mismatch between the coefficients of thermal expansion (CTEs) of the absorber(s) and the functioning layers will accordingly lead to a considerable non-uniformity in the strain distribution (especially at the interfaces) under temperature cycling. In some severe cases, fast periodical temperature changes can accelerate fatigue or even device failure owing to the mechanical delamination of the stack(s). In addition, each layer can also show variations in strain distribution, especially as a function of the film thickness. The impact from the strain also varies by direction; for example, strain along the out-of-plane direction is stronger and more releasable than that in the in-plane direction owing to the presence of adjacent layers along the in-plane direction. This additional strain is concentrated on the defective areas of the interface, leading to delamination after temperature cycling[31]. Compared with fixed temperatures, thermal cycling introduces repetitive mechanical stress and generates dynamic strain owing to the constant expansion and contraction of layers with mismatched CTEs. Therefore, these mechanical and interfacial challenges need to be addressed to improve the durability and reliability of devices under dynamic operating conditions. The introduction of a heterochiral interface has been validated to improve adhesion and mitigate fatigue under repeated thermal cycling (−40 °C to +85 °C for 200 cycles), to address mechanical failures induced by mismatches in the CTEs[66]. Future research can build on such approaches to further enhance the long-term stability of perovskite-based devices.

Impact on the charge transport layers

Characteristics of charge transport materials (CTMs) have a substantial influence on the stability of PSCs during temperature cycling, which brings into question whether the thermal stability of the devices is due to the inherent thermal stability of the CTMs themselves. Indeed, CTMs that possess robust thermal properties are associated with limited interfacial defect generation and have a consistent energy level alignment with the perovskite layer across applied temperature ranges. Using poly[bis(4-phenyl)(2,4,6-trimethylphenyl)amine] (PTAA) instead of spiro-OMeTAD as the CTM, for example, leads to sustained operational efficiency even at elevated temperatures because of its low glass transition temperature[67–69]. Nevertheless, temperature cycles have additional implications on the material and device evolution, which are related to their intrinsic thermal stability[70].

Temperature cycling expedites interlayer material diffusion owing to the dynamic character of the system under consecutive temperature fluctuations. In particular, ion migration is responsible for device instability owing to degradation processes caused by ion rearrangement in

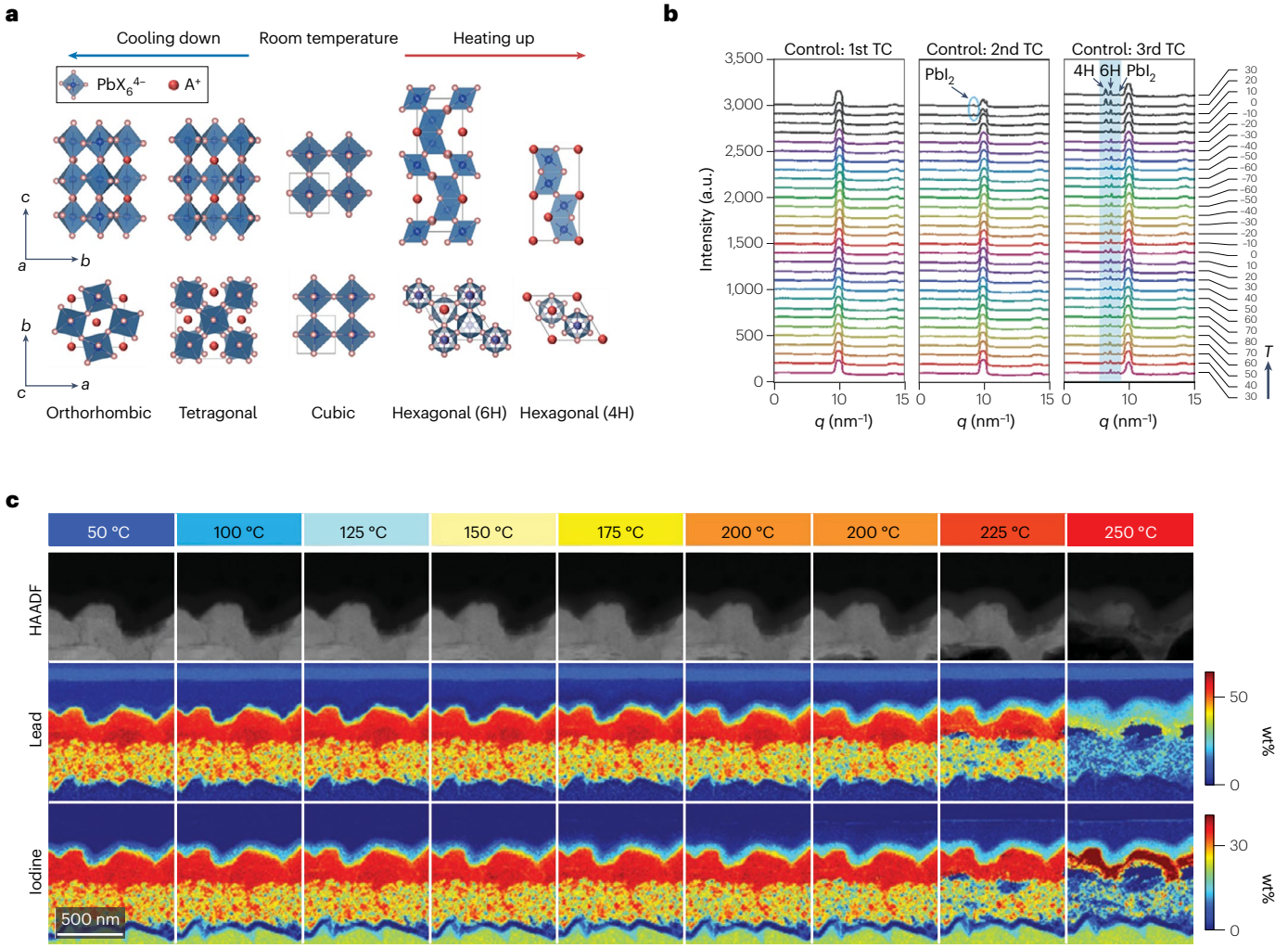

Fig. 2 | Temperature influence on perovskite structure. a, Crystal phases of FAMACs-based perovskites and evolution with temperature (perovskite structure evolution). FAMACs refers to a mixed A-site cation in perovskite composition, as formamidinium (FA), methylammonium (MA) and cesium (Cs). **b**, Temperature-resolved grazing-incidence wide-angle X-ray scattering profiles for FAMACs-based perovskite film with highlighted PbI_2 peak arising (perovskite degradation and phase transition). TC stands for thermal cycling, a process in which the material is subjected to repeated temperature variations. **c**, High-angle annular dark-field (HAADF) images and energy-dispersive X-ray elemental maps for iodine and lead for lamellae perovskite sample obtained after heating at different temperatures (interlayer material degradation). a.u., arbitrary units; *T*, temperature. Part **a** adapted with permission from refs. 137,138, American Chemical Society. Part **b** reprinted with permission from ref. 56, AAAS. Part **c** reprinted from ref. 70, Springer Nature Limited.

the perovskite films and/or redox chemical reactions between migrated ions (especially halides) and active species in the devices[71–74]. In addition, the migration of ions departing from perovskite films (that is, precursor cations and anions) can accelerate the degradation of the transport materials. For example, iodide from the perovskite layer can diffuse across the interface into the adjacent layers. Similarly, metals in the top electrode, such as Ag, Au or Cu, can also diffuse across the buffer and transport layers into the perovskite films[75]. As material diffusion is largely accelerated during temperature cycles, materials with conductivity values that show low dependence on temperature should be chosen to mitigate performance decay.

CTLs should also have CTEs that are aligned with those of the perovskite layer. Within PSCs, the attributes of individual materials in the different layers undergo dynamic fluctuations in response to temperature cycles (Fig. 2c). Disparate CTEs between CTMs and perovskite lead to periodic contractions and expansions at varying rates. When the CTL has a lower CTE than the perovskite (~-3.3×10^{-5} to 8.4×10^{-5} K^{-1}), the CTL constrains the perovskite along the in-plane direction during cooling, resulting in in-plane tensile strain, especially a few nanometres deep in the perovskite layer. Meanwhile, if the CTL has a higher CTE than the perovskite, the opposite can occur. Such interlayer stress could potentially lead to the deformation of chemical bonds and to defect formation at the interfaces, increasing the accumulation and recombination of charge carriers at defect sites and subsequently decreasing the cell performance. In more severe instances, this mismatch may cause delamination and/or fissure propagation, thereby substantially compromising both the efficiency and durability of the devices[76,77]. If the CTL is thin enough, the strain within the perovskite

layer might be negligible compared with the strain exerted by the thicker and stiffer substrate. In this case, the substrate is dominant in controlling the strain in the perovskite. The stress caused by the mismatch in CTE may be balanced by reducing or counteracting the forces between the compressive and tensile layers[78]. For example, using polymer substrates with CTEs closer to that of perovskite layers is an effective strategy for mitigating the stress caused by CTE mismatch[78].

Device performance following temperature cycling

Temperature cycles ultimately lead to changes in the PV performance of devices, which can be reflected in the variations of the different device parameters: PCE, short-circuit current density (J_{SC}), open-circuit voltage (V_{OC}), fill factor (FF) and hysteresis index (HI). The PCE values typically show small variations under temperatures ranging from room temperature to +150 °C (Fig. 3a). As the temperature decreases (from room temperature to −160 °C), however, the PCE begins to decrease, showing an evolution pattern close to that of FF values, whereas the V_{OC} slightly increases. This similarity suggests a tight relationship between the PCE and FF upon the decrease of the temperature, which is likely associated with temperature-related charge extraction events. Unlike conventional solar cells, the increased V_{OC} is not solely attributable to an enlarged bandgap (E_g) at low temperatures, as the E_g of the perovskite decreases slightly with temperature cooling down[63]. It is rather linked to the suppression of trap-assisted non-radiative recombination in both the surface and bulk of the perovskite layer. Meanwhile, the HI considerably increases as the temperature decreases, which is evidenced by comparing the reverse and forward scans of J–V curves (Fig. 3a).

From the viewpoint of thermodynamics, the phase transition from the cubic to the tetragonal phase with lowered temperature enables the effective elimination of intrinsic point defects in perovskite

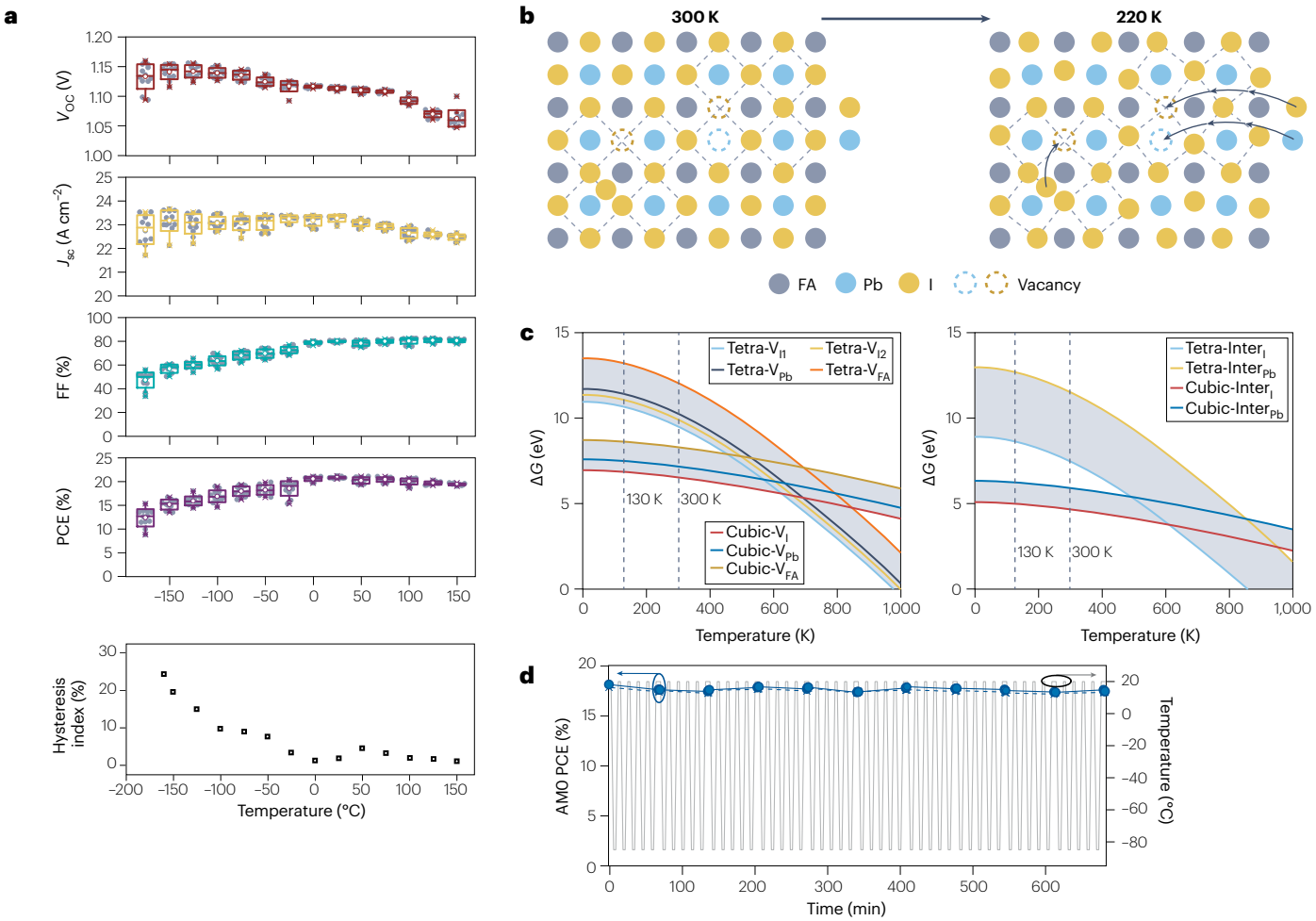

Fig. 3 | The evolution of device performance parameters with temperature cycles. a, Statistical box charts of the open-circuit voltage (V_{OC}), short-circuit current density (J_{SC}), fill factor (FF), power conversion efficiency (PCE) and hysteresis index distribution of perovskite solar cells (PSCs) at different temperatures. The temperature-induced changes in PCE are primarily driven by opposing trends in V_{OC}, with PCE following the same trend as FF and hysteresis index. **b**, A schematic illustration for the self-elimination of intrinsic defects via phase transition. Reducing the temperature aids in the elimination of intrinsic point defects in perovskite materials. **c**, The dependence of ΔG (variation of the Gibbs free energy) for vacancy and interstitial defects on the temperature. Lowering the temperature induces a cubic-to-tetragonal phase transition, increasing defect-formation energy. **d**, Evolution of the PCE of PSCs during 50 thermal cycling between +20 °C and −80 °C at 10 mbar under constant AM0 illumination. The blue symbols correspond to the photovoltaic parameters on the left, and the solid grey lines refer to the temperature on the right. Perovskite devices have reversible performance behaviour upon returning to room temperature. FA, formamidinium. Parts **a** and **d** reprinted from ref. 31, CC BY 4.0. Parts **b** and **c** reprinted with permission from ref. 63, Elsevier.

films, extending the carrier lifetime and enhancing the V_{OC} in devices[63] (Fig. 3b,c). Intriguingly, device performance is recoverable after a limited amount of temperature cycles, and the PCE can even improve after one low-temperature cycle[63]. J_{SC}, V_{OC} and FF remain stable when returned to room temperature after undergoing thermal cycles[31] (Fig. 3d). This resilience may be linked to the restoration of the perovskite structure following temperature fluctuations, which suggests that PSCs have great potential in variable temperature environments, especially those that fluctuate around room temperature. However, as the number of temperature cycles increases, the PCE starts to decline owing to irreversible alterations in the device structure. These alterations include the accumulation of PbI_2, the formation of the hexagonal phase in the

Fig. 4 | Strategies for enhancing photovoltaic performance under thermal cycling. a, Strain relaxation can be achieved via ion incorporation and defect formation. The schematic illustrates the local strain, which is decreased by forming point defects or by doping with small ions. **b**, Relationship between defect formation energy (DFE) and lattice strain. Defect types in $FAPbI_3$ perovskite: FA antisite (I_{FA}), Pb antisite (I_{Pb}), FA vacany (V_{FA}), I vacancy (V_I), Pb vacancy (V_{Pb}) and I interstitial (I_i). Negative strain values correspond to compressive strain, whereas positive values correspond to tensile strain in the out-of-plane direction. **c**, Schematic diagram of charge extraction and recombination at the perovskite/N-doped $PC_{61}BM$ interface at maximum power point at 295 K (+21.85 °C, top) and 180 K (−93.15 °C, bottom). N-type doping enhances the electron transport capability of [60][6,6] phenyl-C61-butyric acid methyl ester (PCBM) at low temperatures and reduces interfacial recombination, enabling the device to work efficiently across a broad temperature range: 1, band-to-band recombination; 2, trap-assisted recombination; blue arrow, interfacial recombination. **d**, Schematic diagram of strain formation process and reduction of strain through buried interface modification with or without a buffer layer between poly(3,4-ethylenedioxythiophene):poly(styrenesulfonate) (PEDOT:PSS) and Sn perovskites. $\Delta d_{//}$ represents the lattice contraction distance in the out-of-plane direction. The buried interfacial modification acts as a buffer layer between the perovskite layer and the hole transport layer, effectively alleviating lattice strain caused by interfacial mismatch during the cooling process. **e**, The temperature-resolved lattice strain for control and target perovskites. For the latter, the perovskite black phase is stabilized using ordered dipoles. The temperature starts from room temperature, heating to +80 °C and then cooling to −60 °C. The progress ends at room temperature. The time per complete cycle is 90 min. The control perovskite undergoes substantial lattice strain evolution during thermal cycling, whereas the target perovskite exhibits strain cycling in a narrower range. **f**, Illustration of how flexible dye self-assembled monolayers (SAMs) alleviate compressive and tensile stresses in perovskite films going through a thermal cycling process. **g**, Normalized temperature cycling test between 290 K (+16.85 °C) and 90 K (−183.15 °C) for the perovskite solar cells with and without a poly(methyl methacrylate) (PMMA) interlayer. The cyclic temperature changes cause tensile and compression strain, which can be alleviated by the PMMA layer. The efficiency of the PMMA-modified device is maintained during temperature cycling. θ, distortion force; e, electrostatic force; E_C, conduction band edge; E_V, valence band edge; FA, formamidinium; PCE, power conversion efficiency. Panel **a** reprinted from ref. 95, Springer Nature Limited. Panel **b** reprinted from ref. 96, Springer Nature Limited. Panel **c** adapted with permission from ref. 139, © 2017 The Authors, published by Wiley-VCH under a CC BY-NC-ND 4.0 License. Panel **d** adapted with permission from ref. 107, Wiley. Panel **e** reprinted with permission from ref. 56, AAAS. Panel **f** reprinted with permission from ref. 140, Springer Nature Limited. Panel **g** reprinted with permission from ref. 85, Elsevier.

perovskite layer, unreleased lattice strain and decreased transport capability and conductivity in CTLs.

Additionally, the evolution of the PV performance with temperature typically remains unaffected by the intensity of the incident light, as suggested through a comparison of irradiation under AM1.5G (standard solar spectrum on Earth's surface, ~1,000 W m^{-2}) and AM0 (solar radiation in outer space, ~1,360 W m^{-2}) conditions[31], or by the voltage. These results suggest that, although additional stress factors such as light and voltage influence the stability of PSCs, operational stability under thermal cycling is mainly determined by the accumulation of irreversible changes in the materials and devices owing to temperature fluctuations. However, testing the cells under a comprehensive combination of all the possible factors should be performed to obtain global insights.

Because perovskite materials with different bandgaps exhibit varying properties, such as thermal stability, ion migration behaviour and mechanical stress tolerance, different responses under temperature cycling are seen. Narrow-bandgap perovskites (<1.5 eV), such as Sn-based or mixed Sn–Pb perovskites, are considered ideal candidates for the bottom cell in tandem solar cells. However, these Sn-containing perovskites are primarily sensitive to oxidation, either from oxygen invasion, acidic poly(3,4-ethylenedioxythiophene):poly(styrenesulfonate) (PEDOT:PSS)-induced I_2 generation, or residual DMSO sourced from the solution processing of the films. These processes can be accelerated under thermal conditions, leading to device failure. Medium-bandgap perovskite materials (1.5–1.7 eV), which are primarily iodide-based (such as $FAPbI_3$), or low-bromide iodide perovskites (when Br <20%), demonstrate relatively good thermal stability and are promising candidates for use in extreme environments with large temperature fluctuations. Although phase transitions and phase separation can still occur during temperature cycling, additive engineering or interfacial modifications can considerably improve their thermal tolerance. For instance, perovskite cells modified with β-poly(1,1-difluoroethylene) exhibited no signs of fatigue after 1,000 h of maximum power point tracking at 75 °C and thermal cycling between −60 °C and +80 °C (ref. 56). Wide-bandgap perovskite materials (>1.7 eV), such as $FAPbBr_3$, exhibit a high population of defect states and numerous ion migration events. However, the accumulation of ions in wide-bandgap perovskite materials can result in phase separation, bandgap shifts and localized electric field failure under temperature cycling, particularly at elevated temperatures[79]. Enhancing thermal expansion compatibility and developing self-healing perovskite materials offer promising approaches to mitigate the degradation of wide-bandgap perovskites under cyclic temperature changes[80].

Strategies to enhance the resilience of perovskite photovoltaics to temperature cycling

There are several strategies to enhance the stability of PSCs under temperature cycling. These strategies encompass stabilizing the phase structure of the perovskites, either by improving the crystallinity of the material or by reducing the lattice strain through the incorporation of buffer materials at grain boundaries, mitigating defects using different modifications approaches and preventing delamination occurring within the perovskite layer itself and at its interfaces with the CTLs by adopting thermally stable and highly conductive CTLs[54,56,81–92].

Stabilizing the perovskite structure

To ensure the stability of PSCs under temperature cycling, the crystalline stability of the perovskite material must be maintained across the specified temperature range, thereby minimizing potential irreversible effects of phase transitions during temperature fluctuations. As a strategy, molecules such as β-poly(1,1-difluoroethylene) with an ordered dipole structure can regulate the crystallization and energy level alignment of the perovskite film. By acting as molecular springs that dynamically respond to stress within the perovskite lattice, these ordered molecules accommodate lattice strain caused by thermal expansion or contraction, effectively stabilizing the crystal structure and mitigating phase transitions. A device made using this strategy showed no signs of fatigue during rapid thermal cycling between −60 °C and +80 °C, highlighting the considerable impact of the ordered dipole structure on the operational stability of PSCs[56]. This result is largely linked to the intrinsic stability of the perovskite materials. For example, in $FAPbI_3$ and $CsPbI_3$, both the large FA^+ ions and the small Cs^+ ions induce distortions in the $[PbX_6]^{4-}$ octahedra, resulting in deviations from the symmetric α-phase (Fig. 4a). This structural distortion is a critical factor

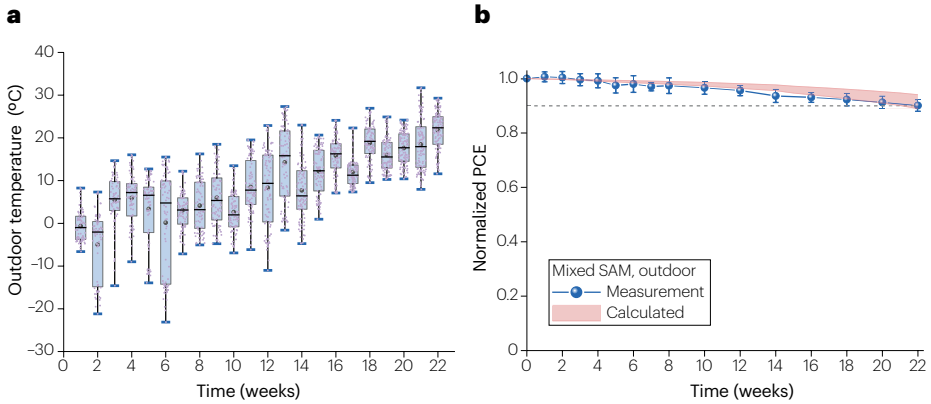

Fig. 5 | Photovoltaic performance under real-world diurnal cycles. a, Outdoor ambient temperature trend. The horizontal line within the box represents the median value, the circle indicates the mean value, the top and bottom bars show the maximum and minimum values and the box itself represents the 25–75% range of the data. **b**, Normalized power conversion efficiency (PCE) evolution of packaged devices under outdoor ageing conditions. The pink band shows the calculated trend. The error bars represent the standard deviations from 14 individual packaged devices. The mixed self-assembled monolayers (SAMs) hole transport layer has enhanced ion-blocking properties that improve interfacial stability, contributing to the outdoor durability of the device. Panels **a** and **b** reprinted from ref. 52, Springer Nature Limited.

underpinning their phase instability[93–96]. By adjusting defect formation energy, lattice strain in perovskites can be controlled (Fig. 4b). Typically, increasing compression stabilizes defects, whereas increasing tension destabilizes them. Consequently, the inactive δ-phases possess the lowest free energy of formation at room temperature, rendering it challenging to achieve stability under constant ambient conditions[97,98]. The ionic structure of the perovskite film is also critical in influencing device thermal stability, which is observed through phase transitions in four standard perovskite materials in devices under thermal cycling between −30 °C and 85 °C (ref. 93). Therefore, for materials such as $MAPbI_3$ and mixed-cation perovskites, characterized by a certain degree of stability at ambient conditions, meticulous attention must be paid to the dependency of potential phase transitions to compositional variations. Notably, it was shown that adjustments in the composition can lower the temperature required for phase transition between the cubic phase and inactive phases at low temperatures, extending their applicability in cold environments[62,63].

Reducing lattice strain

The periphery of the substrate is subject to shear stress, a mechanical effect that is exacerbated by variations in temperature. This phenomenon induces potentially greater displacements within the perovskite lattice, consequently giving rise to lattice distortion or the formation of defects, thereby impacting crucial material properties such as light absorption, charge transport and carrier lifetime (Fig. 4c). Moreover, it can promote alterations in the interface structure between the perovskite and the substrate, thereby influencing interface charge transport dynamics and the sustained efficiency of devices, particularly as they scale up in size[99]. Addressing this issue predominantly revolves around effectively mitigating and dispersing substrate-induced stress while concurrently preserving the uniformity and structural integrity of the perovskite films (Fig. 4d). There is evidence to suggest that rationally applied pressure can instigate phase transitions. Specifically, $MAPbI_3$ can undergo phase transformation at pressures ranging from 0.3 GPa to 0.4 GPa. The residual stress generated during device fabrication can attain 77.7 ± 5.4 MPa under constant room temperature conditions[92]. It was shown that an increase in environmental temperature from −40 °C to 85 °C led to a discernible reduction in residual strain on the surface of the perovskite[92]. Although this strain may not attain the pressure threshold for phase transition, its evolution during thermal cycling can potentially impact phase transition dynamics. This observation further explains why identical perovskite types exhibit varying phase transition temperatures. Incorporating additives into either the perovskite precursor solution or the antisolvent, which is used as quenching agent during wet device fabrication, facilitates the formation of a dense film typified by larger grains owing to the resulting strain in the modified structure. Such dense perovskite films have improved thermal cycle stability. Phase transition is also related to the compactness of the perovskite; in general, the more compact the film is, the more stable it is[56,100–102]. Using a polymer as a buffer against thermomechanical stress at the crystal interfaces (Fig. 4e) improves the perovskite phase stability, suppresses ion diffusion and produces minimal and recoverable tension changes. Using this strategy, fabricated devices could maintain stable PV performance during sustained thermal cycling between −60 °C and +80 °C for 120 cycles[56].

Improving the adhesion at the interfaces

Beyond improving the bulk properties of the perovskite material, it is imperative to regulate detrimental strain and improve the adhesion at the interface between the CTL and the perovskite material to enhance overall device performance. In this sense, an optimal alignment between the CTEs of the perovskite layer and the adjacent layers can prevent fracture and premature delamination. However, maintaining such alignment is challenging, especially considering the simultaneous CTL selection requirements for efficiency optimization. Incorporating molecular interlayers to the stack of the solar cell devices, based on flexible interconnecting molecules to bridge the perovskite and the substrate, could alleviate delamination, thereby contributing to stabilize interfaces and suppress mechanical failure[48,103–106] (Fig. 4f). For instance, introducing a more pliable interlayer, such as poly(methyl methacrylate) (PMMA), dimethylphenethylsulfonium iodide (DMPESI) or ferrocenyl-bis-thiophene-2-carboxylate (FcTc2),

between the perovskite and the CTL, augments stability under thermal cycling conditions[20,54,107] (Fig. 4g). Specifically, PMMA as an interfacial modification layer preserves the crystallinity of the device, which shows almost no efficiency loss after 26 thermal cycles between 290 K and 90 K (ref. 85). These interlayers, interfacing with both the perovskite and CTLs, can modulate phase transition points by passivating defects and alleviating interfacial stress. They can also increase adhesion[104,108], consequently increasing the activation energy of ion migration. Additionally, the fracture energy can serve as a key figure of merit for assessing the interfacial mechanical strength of perovskite devices[109–111]. We believe fracture energy could also be increased through mechanical reinforcement techniques or by integrating materials with higher fracture toughness at the interfaces.

Enhancing the elasticity and mechanical stability of perovskites is another requirement for achieving PSCs that are stable during thermal cycling. The introduction of interface buffer layers could stabilize crystal-to-crystal and layer-to-layer contacts, leading to improved mechanical stability. A mechanistic analysis of how the buffer layer alleviates interfacial stress in the perovskite and enhances the thermal stability of the device could offer valuable insights for developing new buffer layers. As an example, a protonated aminosilane coupling agent, $(OC_2H_5)_3$-Si-$(CH_2)_3$-NH_3Br (PASCA-Br), was used as a buffer layer between TiO_2 and a perovskite layer. The Si end anchors to the TiO_2 layer, improving adhesion, whereas the R-NH_3Br end serves as a structural component to compensate for defects in the octahedral units of the perovskite, reducing lattice distortion. The R-NH_3Br extends the growth sites, helping to release lattice stress, reducing in-plane strain from 1.55% to 0.67% and out-of-plane stress from 1.47% to 0.73%. This strategy effectively mitigates interfacial strain, leading to devices exhibiting higher carrier mobility in a broad temperature range from 223 K to 263 K (ref. 112). In addition, incorporating dense, less penetrable buffer layers and/or less reactive electrodes, such as carbon, or electrodes composed of material(s) capable of forming a diffusion barrier, such as chromium[113,114], would be beneficial to mitigate material interdiffusion.

Photovoltaic performance under real-world diurnal cycles

Evaluating operational stability under field conditions is crucial before projecting perovskite PVs to market[52], as real-world results may differ from laboratory tests[115,116]. This discrepancy was shown, for example, after a 1-year outdoor test in Berlin, where the outdoor operational stability of the device was longer than when measured in conventional laboratory settings[117]. This result may be attributed to the fact that switching between day and night enables devices to sufficiently recover during the night owing to strain relaxation. The change of seasons also has a strong impact on the stability of PSCs; the PCE drops from July to October and November to February, when the weather shows greater temperature changes. PV performance is affected by the exposure to specific absolute temperature values (Fig. 2), but prolonged times and consecutive cycles at high temperatures are much more detrimental for long-term device stability. Meanwhile, other real-world stresses impact device stability[52]. Through a combination of computational simulations and data obtained from outdoor stability tests, it was shown that high temperatures and light strongly determine the stability of PSCs under outdoor conditions (Fig. 5a,b). This dependency can be caused by the photon-catalysed degradation of the perovskite materials and the specific combination and compatibility of the layered materials involved in the devices. In this case, the behaviour observed in laboratory tests correlated with field conditions, enabling the use of indoor accelerated stability tests to predict device performance under outdoor ageing. For the particular case of p–i–n (inverted) PSCs, to improve their stability under temperature cycles and outdoor conditions, a mixture of self-assembled monolayers can be used to improve the interface. Considering the influence of other environmental factors (such as humidity or even rainwater), advancing encapsulation is critical[116]. The PCE of perovskite/silicon tandem solar cells is also strongly dependent on the cyclic nature of operational conditions[118–120].

In particular, we highlight the dependency of the bandgap of the absorber layers on temperature, which leads to variability in the optimal values needed for current matching[118]. First, in perovskite-silicon tandem cells, the optimal bandgap for current matching is about 1.73 eV. However, the c-Si bandgap undergoes a redshift as the temperature increases, whereas the perovskite bandgap undergoes a blueshift, thereby leading to energy level misalignment in the device and impacting its efficiency[118]. Second, when tandem cells are deployed in real-world environments, temperature fluctuations or external forces may induce stress within the thin films. Experimental results have shown that when the temperature drops from 80 °C to 30 °C, the tensile stress in the perovskite film can reach as high as 87.66 MPa (ref. 121). If the compressive stress exceeds the critical stress, it can lead to layer failure or delamination[122]. Moreover, bottom texturization, such as the use of random pyramid textures, substantially improves light coupling efficiency[123]. The top and bottom cells can be

Table 1 | Established ISOS protocols that account for the temperature cycling of perovskite materials and devices

Test ID	Light source	Temperature	Relative humidity	Environment/set-up	Load
ISOS-T-1	None	RT to +65 °C, +85 °C	Ambient	Hot plate/oven	OC
ISOS-T-2	None	RT to +65 °C, +85 °C	Ambient	Oven/env. chamber	OC
ISOS-T-3	None	−40 °C to +85 °C	<55%	Env. chamber	OC
ISOS-LT-1	Solar simulator	Linear or step ramping between RT and +65 °C	Monitored, uncontrolled	Weather chamber	MPP or OC
ISOS-LT-2	Solar simulator	Linear ramping between +5 °C and +65 °C	Monitored, controlled at 50% beyond +40 °C	Env. chamber with a sun simulator	MPP or OC
ISOS-LT-3	Solar simulator	Linear ramping between −25 °C and +65 °C	Monitored, controlled at 50% beyond +40 °C	Env. chamber with sun simulator and freezing	MPP or OC

Env., environmental; ISOS, International Summit on Organic PV Stability; ISOS-LT, ISOS light–humidity–thermal cycling; ISOST, ISOS thermal cycling in the dark; MPP, maximum power point; OC, open-circuit condition; RT, room temperature. Adapted from ref. 18, Springer Nature Limited.

interconnected via a nanocrystalline silicon composite junction, combining low tunnel resistance and high shunt elasticity to fully couple near-infrared light into the c-Si bottom cell[124], thereby addressing the effect of temperature-induced bandgap changes in perovskite and c-Si on tandem cell performance. Using a textured silicon surface structure with no sharp angles can additionally alleviate stress concentration issues during thermal cycling[125]. Furthermore, adjusting the size of A-site ions in the perovskite, such as modifying the content of MA^+, Rb^+ or Cs^+ at the A-site, can help relieve the stress between the perovskite and silicon layers[126,127].

Stability assessment protocols

To better quantify the temperature sensitivity of the performance of PV devices and compare PV parameter variation in different works, the temperature coefficient $\beta_G(T)$, which characterizes the variation of a parameter G (V_{OC}, J_{SC}, FF or PCE) as a function of temperature T, has been introduced[128,129]:

$$\beta_G(T) = \frac{10^6}{G(T_0)} \frac{G(T) - G(T_0)}{T - T_0}, \quad (1)$$

in which T_0 is the room temperature (298.15 K) and the temperature coefficients are expressed in ppm K^{-1}.

As reported, in PSCs, the decline of V_{OC} with increasing temperature is lower than that for silicon solar cells[63]. This result, in theory, suggests that PSCs could present higher operational thermal stability, particularly under temperature cycling conditions.

For the long-term stability test of devices, the perovskite PV research community has constructed test standards based on the International Summit on Organic PV Stability (ISOS)[18,55,130]. As the study of stability under temperature cycling is still in its early stage, applying unified test evaluation procedures is particularly important. There are already some protocols related to measuring devices under temperature cycles, such as ISOI-T-1, ISOI-T-2 and ISOI-T-3 (ref. 18) (Table 1). However, these protocols consider temperature ranges that are too narrow for certain applications and have limited guidelines on other parameters such as heating and cooling rates. The temperature range suggested by the ISOI-T-3 protocol goes from −45 °C to +85 °C, which is enough to simulate most terrestrial applications. Meanwhile, for applications in extreme-temperature earth regions and space environments, a broader cycling temperature range is required[35,131]. In space, the absence of atmosphere and resulting lack of heat transfer can cause the surface temperature of aircraft to fluctuate rapidly and considerably between darkness and sunlight. For these applications, we suggest adopting a wide temperature test range of −160 °C to 150 °C (refs. 31,35). In addition to specifying the temperature range for the thermal cycle, it is also important to establish guidelines for the temperature ramp rate, cooling rate and dwell time at specific temperatures. Rapid heating and cooling rates can generate substantial thermal stress within the cell materials. When temperature changes occur too rapidly, the materials may not expand or contract at the comparable rate, leading to increased mechanical stress that can cause microcracks, interfacial failure or delamination between layers. Therefore, in addition to defining the temperature range for thermal cycling, it is crucial to incorporate heating and cooling rates, as well as specific environmental temperature cycles, into the thermal cycling test protocols. Under light irradiation and at night or when shaded, the simulated accelerated heating or cooling rate could be set broader to provide a better approximation of rapid day–night temperature fluctuations, for instance, an accelerated thermal cycling protocol with a 20 °C min^{-1} ramp rate and a 2-min thermal equilibrium hold between −60 °C and +80 °C. This protocol, in addition to established standards (such as ISOS), should expedite the detection of potential failure modes under fluctuating temperatures, providing faster stability insights and identifying weaknesses within devices and encapsulation materials. Notably, this protocol has demonstrated effectiveness in correlating accelerated perovskite degradation with device thermal cycling stability[56]. Additionally, humidity variations can accelerate material degradation, making it essential to include humidity changes in thermal cycling tests. For instance, in inland basin regions, intense solar radiation during the day leads to rapid temperature increases and a drop in humidity, while at night, radiative cooling causes substantial temperature drops and an increase in humidity. This effect is even more pronounced in extremely dry regions, such as deserts, where fluctuations in temperature and humidity are more extreme. Therefore, we recommend incorporating humidity variation as a key parameter in thermal cycling protocols to more accurately simulate real-world conditions and properly evaluate the impact of temperature and humidity on device performance, ensuring comprehensive test results.

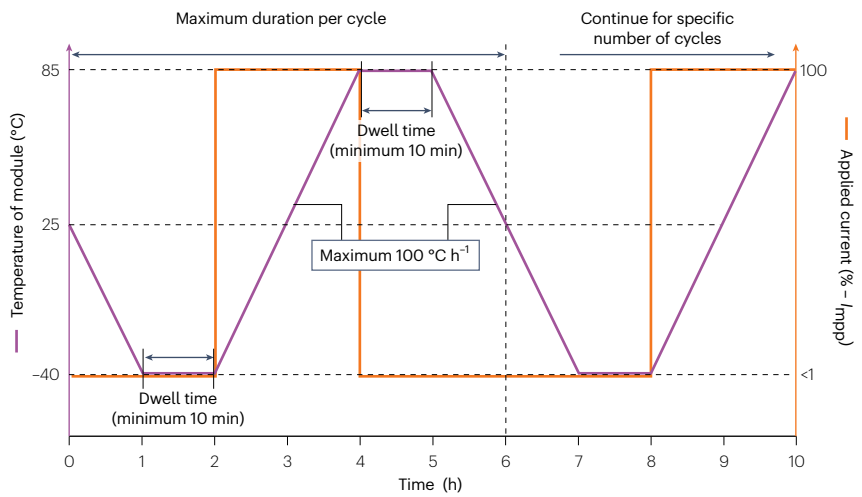

Fig. 6 | Graphic representation of the recommended thermal cycling profile. The modules are suggested to undergo cycling between −40 °C and +85 °C, with a dwell time of minimum 10 min at each temperature extreme. The heating and cooling rates should be maintained between 45 °C h^{-1} and 100 °C h^{-1}, and each cycle should not exceed 6 h. The graphical representation is sketched according to the IEC 61215 standard.

As a reference, Fig. 6 presents a recommended temperature cycle profile ranging from −40 °C to +85 °C, as outlined in the IEC 61215 standard[132,133]. It suggests a cooling and heating rate during the cycles ranging between 45 °C h^{-1} and 100 °C h^{-1} (0.75 °C min^{-1} and 1.67 °C min^{-1}), with a >10-min dwell time, and a duration for one cycle ideally shorter than 6 h. During the thermal process, the applied current can cause local heating in solar cells, potentially leading to high series resistance that exceeds the maximum set temperature. The magnitude of this current depends on the absorber material. When characterizing different properties under temperature cycles, it is advisable to indicate the specific temperature and the number of temperature cycles applied. Additionally, the long-term stability may vary at different temperature intervals[56].

Outlook

The research on accelerated ageing of PSCs through thermal cycling tests has been relatively limited in comparison to constant temperature measurements. Nevertheless, the more and more evident commercialization potential of perovskite PV is gradually encouraging more studies in this direction. Compared with fixed temperatures, temperature cycles have very different impacts on the evolution of the perovskite materials and PV devices. Hence, efforts to unravel the underlying mechanisms of temperature cycling in PSCs and to develop stable and high-efficient perovskite devices under temperature cycles are still needed. Here, we point out four avenues for improving perovskite stability under temperature cycling and provide suggestions for more realistic temperature cycle stability testing in the future.

The first strategy to improve stability would be to explore more effective and robust ligands with multiple anchoring groups, such as polymers, to serve as strain buffers for adjacent layers with different CTEs and inhibit ion migration between the stack layers. Although this approach has been investigated in some studies, its impact under temperature cycling conditions has not been extensively explored, leaving room for further validation in practical scenarios. As a valid strategy to increase the thermal stability of PSCs, achieving robust energy level alignment under temperature cycling is also important to maintain photoconversion efficiency, complementing the function of strain-buffering ligands.

Second, selecting an appropriate CTL is crucial to achieving device stability during temperature cycling. Higher temperatures in the cycling process can have a greater impact on certain organic transport layers, such as Spiro-OMeTAD, which may degrade up to +70 °C (ref. 134). Besides considering the thermal stability of the CTL itself, its CTE should also be considered. It is recommended to choose one that closely matches that of the perovskite layer to prevent delamination between the two layers during temperature cycles. Alternatives such as PTAA offer better thermal stability and closer CTE matching with perovskites, whereas inorganic options such as NiO_x provide exceptional thermal stability and interface robustness. Additionally, self-assembled monolayers, as one of the leading HTL candidates, present challenges under elevated temperatures where bond breakage may occur. Enhancing their binding properties under thermal stress will be a significant milestone in promoting stable perovskite PVs. Evaluating CTLs based on their thermal behaviour, CTE compatibility and durability under cycling conditions is essential for improving the performance and longevity of PSCs.

Third, encapsulation greatly affects the lifetime of devices as it suppresses the internal degradation of volatile species and the external ingression of moisture and reactive species. Important progress has been made in this area, with materials such as ethylene vinyl acetate, polyvinyl butyral and polyisobutylene demonstrating the ability to create effective moisture barriers. These materials are selected based on different characteristics, such as their elastic modulus, morphology and CTE mismatches with the perovskite[48,135,136]. However, challenges remain in achieving encapsulation materials that combine long-term stability with resistance to dynamic thermal cycling. For instance, a rigid encapsulation material possibly departs the PSCs during thermal cycling, leading to mechanical failure. Future research should focus on developing encapsulation systems with enhanced barrier properties, self-healing mechanisms and better compatibility with perovskite layers to address delamination and moisture ingress over time. Therefore, suitable encapsulant materials and techniques are highly needed to enhance thermal cycling stability and improve the commercial viability of the device by reducing the impact of temperature cycling on the entire device. It is also important to conduct thermal cycling tests on fully encapsulated devices to evaluate and study the mechanisms involved during temperature cycling.

Finally, the decomposition mechanism of PSCs under temperature cycles remains underexplored. To gain a better understanding of its behaviour, it is crucial to use consistent and uniform testing methods. Given that high temperatures typically coincide with sunlight exposure, and low temperatures normally occur at night-time, it would be more meaningful to study the working performance of PSCs at high temperatures and their storage and/or self-healing performance at low or room temperatures within thermal cycling. This approach would provide valuable insights into the behaviour and stability of PSCs under realistic operating conditions. By examining the performance of solar devices during both high-temperature operation and low-temperature storage and/or recovery, researchers can gather comprehensive knowledge relevant to practical applications and address the challenges associated with temperature cycling more effectively. Additionally, to better study the working mechanism of PSCs in real life, other stress combination, such as temperature with humidity, bias or atmosphere, should be considered in future research.

Published online: 19 February 2025

References

1. Green, M. A., Ho-Baillie, A. & Snaith, H. J. The emergence of perovskite solar cells. *Nat. Photon.* **8**, 506–514 (2014).
2. Saliba, M. et al. Incorporation of rubidium cations into perovskite solar cells improves photovoltaic performance. *Science* **354**, 206–209 (2016).
3. De Wolf, S. et al. Organometallic halide perovskites: sharp optical absorption edge and its relation to photovoltaic performance. *J. Phys. Chem. Lett.* **5**, 1035–1039 (2014).
4. Wu, L. et al. Stabilization of inorganic perovskite solar cells with a 2D Dion–Jacobson passivating layer. *Adv. Mater.* **35**, 2304150 (2023).
5. Huang, W., Bu, T., Huang, F. & Cheng, Y. B. Stabilizing high efficiency perovskite solar cells with 3D–2D heterostructures. *Joule* **4**, 975–979 (2020).
6. Saliba, M., Correa-Baena, J.-P., Grätzel, M., Hagfeldt, A. & Abate, A. Perovskite solar cells: from the atomic level to film quality and device performance. *Angew. Chem. Int. Ed.* **57**, 2554–2569 (2018).
7. Liu, D. & Kelly, T. L. Perovskite solar cells with a planar heterojunction structure prepared using room-temperature solution processing techniques. *Nat. Photon.* **8**, 133–138 (2014).
8. Stranks, S. D. & Snaith, H. J. Metal-halide perovskites for photovoltaic and light-emitting devices. *Nat. Nanotechnol.* **10**, 391–402 (2015).
9. Liu, M., Johnston, M. B. & Snaith, H. J. Efficient planar heterojunction perovskite solar cells by vapour deposition. *Nature* **501**, 395–398 (2013).
10. Nandi, P. et al. $CH_3NH_3PbI_3$, a potential solar cell candidate: structural and spectroscopic investigations. *J. Phys. Chem. A* **120**, 9732–9739 (2016).
11. Liu, S. et al. Buried interface molecular hybrid for inverted perovskite solar cells. *Nature* **632**, 536–542 (2024).
12. Peters, I. M., Rodríguez Gallegos, C. D., Lüer, L., Hauch, J. A. & Brabec, C. J. Practical limits of multijunction solar cells. *Prog. Photovolt.* **31**, 1006–1015 (2023).
13. McMeekin, D. P. et al. A mixed-cation lead mixed-halide perovskite absorber for tandem solar cells. *Science* **351**, 151–155 (2016).

14. Stranks, S. D. et al. Electron–hole diffusion lengths exceeding 1 micrometer in an organometal trihalide perovskite absorber. *Science* **342**, 341–344 (2013).
15. Green, M. A. et al. Solar cell efficiency tables (version 64). *Prog. Photovolt.* **32**, 425–441 (2024).
16. Luo, L. et al. Stabilization of 3D/2D perovskite heterostructures via inhibition of ion diffusion by cross-linked polymers for solar cells with improved performance. *Nat. Energy* **8**, 294–303 (2023).
17. Turren-Cruz, S.-H., Hagfeldt, A. & Saliba, M. Methylammonium-free, high-performance, and stable perovskite solar cells on a planar architecture. *Science* **362**, 449–453 (2018).
18. Khenkin, M. V. et al. Consensus statement for stability assessment and reporting for perovskite photovoltaics based on ISOS procedures. *Nat. Energy* **5**, 35–49 (2020).
19. Jeronimo-Rendon, J. J. et al. Robust multi-halide methylammonium-free perovskite solar cells on an inverted architecture. *Adv. Funct. Mater.* **34**, 2313928 (2024).
20. Li, Z. et al. Organometallic-functionalized interfaces for highly efficient inverted perovskite solar cells. *Science* **376**, 416–420 (2022).
21. Chen, R. et al. Reduction of bulk and surface defects in inverted methylammonium- and bromide-free formamidinium perovskite solar cells. *Nat. Energy* **8**, 839–849 (2023).
22. Yang, Y. et al. Inverted perovskite solar cells with over 2,000 h operational stability at 85 °C using fixed charge passivation. *Nat. Energy* **9**, 37–46 (2023).
23. Li, G. et al. Managing excess lead iodide with functionalized oxo-graphene nanosheets for stable perovskite solar cells. *Angew. Chem. Int. Ed.* **135**, e202307395 (2023).
24. Wang, M. et al. Ammonium cations with high pKa in perovskite solar cells for improved high-temperature photostability. *Nat. Energy* **8**, 1229–1239 (2023).
25. Li, H. et al. 2D/3D heterojunction engineering at the buried interface towards high-performance inverted methylammonium-free perovskite solar cells. *Nat. Energy* **8**, 946–955 (2023).
26. Jiang, Q. et al. Surface reaction for efficient and stable inverted perovskite solar cells. *Nature* **611**, 278–283 (2022).
27. Zhu, K. & Stranks, S. D. Energy spotlight. *ACS Energy Lett.* **7**, 1862–1863 (2022).
28. Park, S. M. et al. Engineering ligand reactivity enables high-temperature operation of stable perovskite solar cells. *Science* **381**, 209–215 (2023).
29. Li, C. et al. Rational design of Lewis base molecules for stable and efficient inverted perovskite solar cells. *Science* **379**, 690–694 (2023).
30. Peng, W. et al. Reducing nonradiative recombination in perovskite solar cells with a porous insulator contact. *Science* **379**, 683–690 (2023).
31. Li, G. et al. Structure and performance evolution of perovskite solar cells under extreme temperatures. *Adv. Energy Mater.* **12**, 2202887 (2022).
32. Sharma, N. et al. Solar power forecasting beneath diverse weather conditions using GD and LM-artificial neural networks. *Sci. Rep.* **13**, 8517 (2023).
33. Akbulatov, A. F. et al. Effect of electron-transport material on light-induced degradation of inverted planar junction perovskite solar cells. *Adv. Energy Mater.* **7**, 1700476 (2017).
34. De Bastiani, M. et al. Toward stable monolithic perovskite/silicon tandem photovoltaics: a six-month outdoor performance study in a hot and humid climate. *ACS Energy Lett.* **6**, 2944–2951 (2021).
35. Tu, Y. et al. Perovskite solar cells for space applications: progress and challenges. *Adv. Mater.* **33**, 2006545 (2021).
36. Brown, C. R., Eperon, G. E., Whiteside, V. R. & Sellers, I. R. Potential of high-stability perovskite solar cells for low-intensity–low-temperature (LILT) outer planetary space missions. *ACS Appl. Energy Mater.* **2**, 814–821 (2019).
37. Park, S. M. et al. Low-loss contacts on textured substrates for inverted perovskite solar cells. *Nature* **624**, 289–294 (2023).
38. Reb, L. K. et al. Perovskite and organic solar cells on a rocket flight. *Joule* **4**, 1880–1892 (2020).
39. Barbé, J. et al. In situ investigation of perovskite solar cells' efficiency and stability in a mimic stratospheric environment for high-altitude pseudo-satellites. *J. Mater. Chem. C* **8**, 1715–1721 (2020).
40. Romano, V., Agresti, A., Verduci, R. & D'Angelo, G. Advances in perovskites for photovoltaic applications in space. *ACS Energy Lett.* **7**, 2490–2514 (2022).
41. Yang, J., Bao, Q., Shen, L. & Ding, L. Potential applications for perovskite solar cells in space. *Nano Energy* **76**, 105019 (2020).
42. Ma, Q., Liao, S., Ma, Y., Chu, Y. & Wang, Y. An ultra-low-temperature elastomer with excellent mechanical performance and solvent resistance. *Adv. Mater.* **33**, 2102096 (2021).
43. Panteli, M. & Mancarella, P. Influence of extreme weather and climate change on the resilience of power systems: impacts and possible mitigation strategies. *Electr. Power Syst. Res.* **127**, 259–270 (2015).
44. Al-Shahri, O. A. et al. Solar photovoltaic energy optimization methods, challenges and issues: a comprehensive review. *J. Clean. Prod.* **284**, 125465 (2021).
45. Gernaat, D. E. H. J. et al. Climate change impacts on renewable energy supply. *Nat. Clim. Change* **11**, 119–125 (2021).
46. Tu, Y. et al. Mixed-cation perovskite solar cells in space. *Sci. China Phys. Mech. Astron.* **62**, 974221 (2019).
47. Wang, X. et al. Elimination of charge accumulation by a self-assembled cocrystal interlayer for efficient and stable perovskite solar cells. *Energy Environ. Sci.* **17**, 569–579 (2024).
48. Cheacharoen, R. et al. Design and understanding of encapsulated perovskite solar cells to withstand temperature cycling. *Energy Environ. Sci.* **11**, 144–150 (2018).
49. Guo, R. et al. Degradation mechanisms of perovskite solar cells under vacuum and one atmosphere of nitrogen. *Nat. Energy* **6**, 977–986 (2021).
50. Domanski, K., Alharbi, E. A., Hagfeldt, A., Grätzel, M. & Tress, W. Systematic investigation of the impact of operation conditions on the degradation behaviour of perovskite solar cells. *Nat. Energy* **3**, 61–67 (2018).
51. Zhou, Y., Herz, L. M., Jen, A. K. Y. & Saliba, M. Advances and challenges in understanding the microscopic structure–property–performance relationship in perovskite solar cells. *Nat. Energy* **7**, 794–807 (2022).
52. Jiang, Q. et al. Towards linking lab and field lifetimes of perovskite solar cells. *Nature* **623**, 313–318 (2023).
53. Li, X. et al. Iodine-trapping strategy for light-heat stable inverted perovskite solar cells under ISOS protocols. *Energy Environ. Sci.* **16**, 6071–6077 (2023).
54. Suo, J. et al. Multifunctional sulfonium-based treatment for perovskite solar cells with less than 1% efficiency loss over 4,500-h operational stability tests. *Nat. Energy* **9**, 172–183 (2024).
55. Khenkin, M. et al. Light cycling as a key to understanding the outdoor behaviour of perovskite solar cells. *Energy Environ. Sci.* **17**, 602–610 (2024).
56. Li, G. et al. Highly efficient p–i–n perovskite solar cells that endure temperature variations. *Science* **379**, 399–403 (2023).
57. Li, Z., Park, J. S. & Walsh, A. Evolutionary exploration of polytypism in lead halide perovskites. *Chem. Sci.* **12**, 12165–12173 (2021).
58. Domanski, K. et al. Migration of cations induces reversible performance losses over day/night cycling in perovskite solar cells. *Energy Environ. Sci.* **10**, 604–613 (2017).
59. Hoang, M. T., Yang, Y., Tuten, B. & Wang, H. Are metal halide perovskite solar cells ready for space applications? *J. Phys. Chem. Lett.* **13**, 2908–2920 (2022).
60. Juarez-Perez, E. J., Hawash, Z., Raga, S. R., Ono, L. K. & Qi, Y. Thermal degradation of $CH_3NH_3PbI_3$ perovskite into NH_3 and CH_3I gases observed by coupled thermogravimetry–mass spectrometry analysis. *Energy Environ. Sci.* **9**, 3406–3410 (2016).
61. Ava, T. T., Al Mamun, A., Marsillac, S. & Namkoong, G. A review: thermal stability of methylammonium lead halide based perovskite solar cells. *Appl. Sci.* **9**, 188 (2019).
62. Weber, O. J., Charles, B. & Weller, M. T. Phase behaviour and composition in the formamidinium–methylammonium hybrid lead iodide perovskite solid solution. *J. Mater. Chem. A* **4**, 15375–15382 (2016).
63. Chen, Y. et al. Self-elimination of intrinsic defects improves the low-temperature performance of perovskite photovoltaics. *Joule* **4**, 1961–1976 (2020).
64. Meng, W. et al. Revealing the strain-associated physical mechanisms impacting the performance and stability of perovskite solar cells. *Joule* **6**, 458–475 (2022).
65. Wu, J. et al. Strain in perovskite solar cells: origins, impacts and regulation. *Natl Sci. Rev.* **8**, nwab047 (2021).
66. Duan, T. et al. Chiral-structured heterointerfaces enable durable perovskite solar cells. *Science* **384**, 878–884 (2024).
67. Malinauskas, T. et al. Enhancing thermal stability and lifetime of solid-state dye-sensitized solar cells via molecular engineering of the hole-transporting material spiro-OMeTAD. *ACS Appl. Mater. Interfaces* **7**, 11107–11116 (2015).
68. Zhao, X., Kim, H.-S., Seo, J.-Y. & Park, N.-G. Effect of selective contacts on the thermal stability of perovskite solar cells. *ACS Appl. Mater. Interfaces* **9**, 7148–7153 (2017).
69. Jena, A. K., Numata, Y., Ikegami, M. & Miyasaka, T. Role of spiro-OMeTAD in performance deterioration of perovskite solar cells at high temperature and reuse of the perovskite films to avoid Pb-waste. *J. Mater. Chem. A* **6**, 2219–2230 (2018).
70. Divitini, G. et al. In situ observation of heat-induced degradation of perovskite solar cells. *Nat. Energy* **1**, 15012–15012 (2016).
71. Snaith, H. J. et al. Anomalous hysteresis in perovskite solar cells. *J. Phys. Chem. Lett.* **5**, 1511–1515 (2014).
72. Unger, E. L. et al. Hysteresis and transient behavior in current–voltage measurements of hybrid-perovskite absorber solar cells. *Energy Environ. Sci.* **7**, 3690–3698 (2014).
73. Tress, W. et al. Understanding the rate-dependent *J–V* hysteresis, slow time component, and aging in $CH_3NH_3PbI_3$ perovskite solar cells: the role of a compensated electric field. *Energy Environ. Sci.* **8**, 995–1004 (2015).
74. Yang, T.-Y., Gregori, G., Pellet, N., Grätzel, M. & Maier, J. The significance of ion conduction in a hybrid organic–inorganic lead-iodide-based perovskite photosensitizer. *Angew. Chem. Int. Ed.* **54**, 7905–7910 (2015).
75. Zhang, D., Li, D., Hu, Y., Mei, A. & Han, H. Degradation pathways in perovskite solar cells and how to meet international standards. *Commun. Mater.* **3**, 58 (2022).
76. Ma, S. et al. Development of encapsulation strategies towards the commercialization of perovskite solar cells. *Energy Environ. Sci.* **15**, 13–55 (2022).
77. Dong, Q. et al. Interpenetrating interfaces for efficient perovskite solar cells with high operational stability and mechanical robustness. *Nat. Commun.* **12**, 973 (2021).
78. McAndrews, G. R. et al. Why perovskite thermal stress is unaffected by thin contact layers. *Adv. Energy Mater.* **14**, 2400764 (2024).
79. Chen, C. et al. Arylammonium-assisted reduction of the open-circuit voltage deficit in wide-bandgap perovskite solar cells: the role of suppressed ion migration. *ACS Energy Lett.* **5**, 2560–2568 (2020).
80. Liu, J. et al. Mitigating deep-level defects through a self-healing process for highly efficient wide-bandgap inorganic $CsPbI_{3-x}Br_x$ perovskite photovoltaics. *J. Mater. Chem. A* **10**, 17237–17245 (2022).
81. Shi, P. et al. Oriented nucleation in formamidinium perovskite for photovoltaics. *Nature* **620**, 323–327 (2023).
82. Tan, Q. et al. Inverted perovskite solar cells using dimethylacridine-based dopants. *Nature* **620**, 545–551 (2023).

83. Li, F. et al. Hydrogen-bond-bridged intermediate for perovskite solar cells with enhanced efficiency and stability. *Nat. Photon.* **17**, 478–484 (2023).
84. Jiang, Q. et al. Compositional texture engineering for highly stable wide-bandgap perovskite solar cells. *Science* **378**, 1295–1300 (2022).
85. Qiu, W. et al. Low-temperature robust $MAPbI_3$ perovskite solar cells with power conversion efficiency exceeding 22.4%. *Chem. Eng. J.* **468**, 143656 (2023).
86. Wang, S. et al. In situ self-elimination of defects via controlled perovskite crystallization dynamics for high-performance solar cells. *Adv. Mater.* **35**, 2305314 (2023).
87. You, S. et al. Bifunctional hole-shuttle molecule for improved interfacial energy level alignment and defect passivation in perovskite solar cells. *Nat. Energy* **8**, 515–525 (2023).
88. Zhang, C. et al. Crystallization manipulation and holistic defect passivation toward stable and efficient inverted perovskite solar cells. *Energy Environ. Sci.* **16**, 3825–3836 (2023).
89. Liu, C. et al. Bimolecularly passivated interface enables efficient and stable inverted perovskite solar cells. *Science* **382**, 810–815 (2023).
90. Yu, S. et al. Homogenized NiO_x nanoparticles for improved hole transport in inverted perovskite solar cells. *Science* **382**, 1399–1404 (2023).
91. Wang, C. et al. Enhancing the inherent stability of perovskite solar cells through chalcogenide-halide combinations. *Energy Environ. Sci.* **17**, 1368–1386 (2024).
92. Wang, H. et al. Interfacial residual stress relaxation in perovskite solar cells with improved stability. *Adv. Mater.* **31**, 1904408 (2019).
93. He, J. et al. Influence of phase transition on stability of perovskite solar cells under thermal cycling conditions. *Sol. Energy* **188**, 312–317 (2019).
94. Yang, B. et al. Strain effects on halide perovskite solar cells. *Chem. Soc. Rev.* **51**, 7509–7530 (2022).
95. Saidaminov, M. I. et al. Suppression of atomic vacancies via incorporation of isovalent small ions to increase the stability of halide perovskite solar cells in ambient air. *Nat. Energy* **3**, 648–654 (2018).
96. Deger, C., Tan, S., Houk, K. N., Yang, Y. & Yavuz, I. Lattice strain suppresses point defect formation in halide perovskites. *Nano Res.* **15**, 5746–5751 (2022).
97. Kim, G. et al. Impact of strain relaxation on performance of α-formamidinium lead iodide perovskite solar cells. *Science* **370**, 108–112 (2020).
98. Lee, J.-H. et al. Resolving the physical origin of octahedral tilting in halide perovskites. *Chem. Mater.* **28**, 4259–4266 (2016).
99. Wang, L. et al. $[PbX6]^{4-}$ modulation and organic spacer construction for stable perovskite solar cells. *Energy Environ. Sci.* **15**, 4470–4510 (2022).
100. Shi, Y. & Chu, L. Dipole polymer-coated crystalline grains to endure temperature variations of perovskite photovoltaics. *Matter* **6**, 1063–1065 (2023).
101. Luo, D., Su, R., Zhang, W., Gong, Q. & Zhu, R. Minimizing non-radiative recombination losses in perovskite solar cells. *Nat. Rev. Mater.* **5**, 44–60 (2020).
102. Zhang, Y. et al. Improved fatigue behaviour of perovskite solar cells with an interfacial starch–polyiodide buffer layer. *Nat. Photon.* **17**, 1066–1073 (2023).
103. Dai, Z. et al. Interfacial toughening with self-assembled monolayers enhances perovskite solar cell reliability. *Science* **372**, 618–622 (2021).
104. Dai, Z. et al. Connecting interfacial mechanical adhesion, efficiency, and operational stability in high performance inverted perovskite solar cells. *ACS Energy Lett.* **9**, 1880–1887 (2024).
105. Watson, B. L., Rolston, N., Printz, A. D. & Dauskardt, R. H. Scaffold-reinforced perovskite compound solar cells. *Energy Environ. Sci.* **10**, 2500–2508 (2017).
106. Rolston, N. et al. Rapid open-air fabrication of perovskite solar modules. *Joule* **4**, 2675–2692 (2020).
107. Teng, T. Y. et al. Electronically manipulated molecular strategy enabling highly efficient tin perovskite photovoltaics. *Angew. Chem.* **136**, e202318133 (2024).
108. Dai, Z. et al. Dual-interface-reinforced flexible perovskite solar cells for enhanced performance and mechanical reliability. *Adv. Mater.* **34**, 2205301 (2022).
109. Hilt, F. et al. Rapid route to efficient, scalable, and robust perovskite photovoltaics in air. *Energy Environ. Sci.* **11**, 2102–2113 (2018).
110. Liu, D. et al. Strain analysis and engineering in halide perovskite photovoltaics. *Nat. Mater.* **20**, 1337–1346 (2021).
111. Dai, Z. & Padture, N. P. Challenges and opportunities for the mechanical reliability of metal halide perovskites and photovoltaics. *Nat. Energy* **8**, 1319–1327 (2023).
112. Zhang, C.-C. et al. Perovskite films with reduced interfacial strains via a molecular-level flexible interlayer for photovoltaic application. *Adv. Mater.* **32**, 2001479 (2020).
113. Kaltenbrunner, M. et al. Flexible high power-per-weight perovskite solar cells with chromium oxide–metal contacts for improved stability in air. *Nat. Mater.* **14**, 1032–1039 (2015).
114. Domanski, K. et al. Not all that glitters is gold: metal-migration-induced degradation in perovskite solar cells. *ACS Nano* **10**, 6306–6314 (2016).
115. Tress, W. et al. Performance of perovskite solar cells under simulated temperature-illumination real-world operating conditions. *Nat. Energy* **4**, 568–574 (2019).
116. Zhang, G. et al. Shellac protects perovskite solar cell modules under real-world conditions. *Joule* **8**, 496–508 (2024).
117. Li, J. et al. Ink design enabling slot-die coated perovskite solar cells with >22% power conversion efficiency, micro-modules, and 1 year of outdoor performance evaluation. *Adv. Energy Mater.* **13**, 2203898 (2023).
118. Aydin, E. et al. Interplay between temperature and bandgap energies on the outdoor performance of perovskite/silicon tandem solar cells. *Nat. Energy* **5**, 851–859 (2020).
119. Xie, H. et al. Decoupling the effects of defects on efficiency and stability through phosphonates in stable halide perovskite solar cells. *Joule* **5**, 1246–1266 (2021).
120. Babics, M. et al. One-year outdoor operation of monolithic perovskite/silicon tandem solar cells. *Cell Rep. Phys. Sci.* **4**, 101280 (2023).
121. Liu, K., Wang, Z., Qu, S. & Ding, L. Stress and strain in perovskite/silicon tandem solar cells. *Nano-Micro Lett.* **15**, 59 (2023).
122. Dailey, M., Li, Y. & Printz, A. D. Residual film stresses in perovskite solar cells: origins, effects, and mitigation strategies. *ACS Omega* **6**, 30214–30223 (2021).
123. Sahli, F. et al. Fully textured monolithic perovskite/silicon tandem solar cells with 25.2% power conversion efficiency. *Nat. Mater.* **17**, 820–826 (2018).
124. Sahli, F. et al. Improved optics in monolithic perovskite/silicon tandem solar cells with a nanocrystalline silicon recombination junction. *Adv. Energy Mater.* **8**, 1701609 (2018).
125. Chen, B. et al. Blade-coated perovskites on textured silicon for 26%-efficient monolithic perovskite/silicon tandem solar cells. *Joule* **4**, 850–864 (2020).
126. Jiang, J. et al. Synergistic strain engineering of perovskite single crystals for highly stable and sensitive X-ray detectors with low-bias imaging and monitoring. *Nat. Photon.* **16**, 575–581 (2022).
127. Roß, M. et al. Co-evaporated formamidinium lead iodide based perovskites with 1000 h constant stability for fully textured monolithic perovskite/silicon tandem solar cells. *Adv. Energy Mater.* **11**, 2101460 (2021).
128. Dupré, O., Vaillon, R. & Green, M. A. Physics of the temperature coefficients of solar cells. *Sol. Energy Mater. Sol. Cell* **140**, 92–100 (2015).
129. Babics, M., Bristow, H., Pininti, A. R., Allen, T. G. & De Wolf, S. Temperature coefficients of perovskite/silicon tandem solar cells. *ACS Energy Lett.* **8**, 3013–3015 (2023).
130. Cheacharoen, R. et al. Damp heat, temperature cycling and UV stress testing of encapsulated perovskite photovoltaic cells. In *2018 IEEE 7th World Conference on Photovoltaic Energy Conversion* (*WCPEC*) 3498–3502 (IEEE, 2018).
131. Delmas, W. et al. Evaluation of hybrid perovskite prototypes after 10-month space flight on the International Space Station. *Adv. Energy Mater.* **13**, 2203920 (2023).
132. Jošt, M. et al. Perovskite solar cells go outdoors: field testing and temperature effects on energy yield. *Adv. Energy Mater.* **10**, 2000454 (2020).
133. Reese, M. O. et al. Consensus stability testing protocols for organic photovoltaic materials and devices. *Sol. Energy Mater. Sol. Cell* **95**, 1253–1267 (2011).
134. Rombach, F. M., Haque, S. A. & Macdonald, T. J. Lessons learned from spiro-OMeTAD and PTAA in perovskite solar cells. *Energy Environ. Sci.* **14**, 5161–5190 (2021).
135. Cheacharoen, R. et al. Encapsulating perovskite solar cells to withstand damp heat and thermal cycling. *Sustain. Energy Fuels* **2**, 2398–2406 (2018).
136. Jiao, H. et al. Metal halide perovskite solar module encapsulation using polyolefin elastomers: the role of morphology in preventing delamination. *PRX Energy* **3**, 023013 (2024).
137. Gratia, P. et al. The many faces of mixed ion perovskites: unraveling and understanding the crystallization process. *ACS Energy Lett.* **2**, 2686–2693 (2017).
138. Thind, A. S., Huang, X., Sun, J. & Mishra, R. First-principles prediction of a stable hexagonal phase of $CH_3NH_3PbI_3$. *Chem. Mater.* **29**, 6003–6011 (2017).
139. Shao, S. et al. Efficient perovskite solar cells over a broad temperature window: the role of the charge carrier extraction. *Adv. Energy Mater.* **7**, 1701305 (2017).
140. Isikgor, F. H. et al. Molecular engineering of contact interfaces for high-performance perovskite solar cells. *Nat. Rev. Mater.* **8**, 89–108 (2023).

Acknowledgements

This Perspective is supported by the European Research Council (ERC) under the European Union's Horizon 2020 research and innovation programme (grant agreement no. 804519), the European Union's Horizon Europe research and innovation programme under grant agreement no. 101075330 of the NEXUS project and the Marie Skłodowska Curie Actions Postdoc Fellow (UKRI Guarantee, grant no. EP/Y029216/1). S.-H.T.-C. thanks the funding support of the Ministry of Science and Innovation of Spain under Ayudas Ramón y Cajal (RYC2022-035578-I). J.P. acknowledges support from Energy for Future — E4F Postdoctoral fellowship programme H2020-MSCA-COFUND-2020 (101034297). M. Saliba thanks the German Research Foundation (DFG) for funding (SPP2196, 431314977/GRK 2642); GRK: 'funded by the Deutsche Forschungsgemeinschaft (DFG, German Research Foundation) — 431314977/GRK2642'. M. Saliba acknowledges funding from the European Union under the Horizon Europe programme (ERC, LOCAL-HEAT, grant agreement no. 101041809). M. Saliba acknowledges funding from the German Bundesministerium für Bildung and Forschung (BMBF), project 'NETPEC' (01LS2103E). Views and opinions expressed are, however, those of the author(s) only and do not necessarily reflect those of the European Union or the European Research Council. Neither the European Union nor the granting authority can be held responsible for them.

Author contributions

L.W., S.H., F.Y. and G.L. contributed to the writing and editing of this manuscript. L.W. and G.L. prepared the first draft. G.L. and M.L. contributed to the discussion of content and writing. A.A. contributed to the discussion and review of the manuscript. G.L., J.P., M.L. and A.A. supervised the project. S.H., F.Y., J.W., W.Z., J.J.J.-R., J.P. and S.-H.T.-C. contributed to suggestions and revised the manuscript. M. Saba, M. Saliba and M.K.N. reviewed and edited the manuscript. All authors contributed their expertise and participated in revision rounds of the manuscript.

Competing interests

The authors declare no competing interests.

Additional information
Peer review information *Nature Reviews Materials* thanks Michael McGehee and the other, anonymous, reviewer(s) for their contribution to the peer review of this work.

[1]Helmholtz-Zentrum Berlin für Materialien und Energie GmbH, Berlin, Germany. [2]Department of Physics, Università degli Studi di Cagliari, Monserrato, Italy. [3]Clarendon Laboratory, Department of Physics, University of Oxford, Oxford, UK. [4]Key Lab for Special Functional Materials of Ministry of Education, National & Local Joint Engineering Research Center for High-efficiency Display and Lighting Technology, School of Nanoscience and Materials Engineering, Collaborative Innovation Center of Nano Functional Materials and Applications, Henan University, Kaifeng, P. R. China. [5]College of Physics, Henan Key Laboratory of Advanced Semiconductor & Functional Device Integration, Henan Normal University, Xinxiang, P. R. China. [6]Institute of Chemical Sciences and Engineering, École Polytechnique Fédérale de Lausanne (EPFL), Lausanne, Switzerland. [7]School of Materials Science and Engineering, Southeast University, Nanjing, P. R. China. [8]Institute for Photovoltaics (ipv), University of Stuttgart, Stuttgart, Germany. [9]Instituto de Ciencia de los Materiales (ICMUV), Universidad de Valencia, Paterna, Spain. [10]Helmholtz Young Investigator Group FRONTRUNNER, IEK5-Photovoltaics Forschungszentrum Jülich, Jülich, Germany. [11]Polymat, University of the Basque Country UPV/EHU, Donostia-San Sebastian, Spain. [12]Department of Chemistry, Bielefeld University, Bielefeld, Germany. [13]These authors contributed equally: Luyan Wu, Shuaifeng Hu, Feng Yang.